

This work was written as part of one of the author's official duties as an Employee of the United States Government and is therefore a work of the United States Government. In accordance with 17 U.S.C. 105, no copyright protection is available for such works under U.S. Law.

Public Domain Mark 1.0

<https://creativecommons.org/publicdomain/mark/1.0/>

Access to this work was provided by the University of Maryland, Baltimore County (UMBC) ScholarWorks@UMBC digital repository on the Maryland Shared Open Access (MD-SOAR) platform.

Please provide feedback

Please support the ScholarWorks@UMBC repository by emailing scholarworks-group@umbc.edu and telling us what having access to this work means to you and why it's important to you. Thank you.

Limitations of multispacecraft data techniques in measuring wave number spectra of space plasma turbulence

F. Sahraoui,^{1,2} G. Belmont,² M. L. Goldstein,¹ and L. Rezeau²

Received 4 August 2009; revised 10 October 2009; accepted 20 October 2009; published 10 April 2010.

[1] Unambiguous determination of spatial properties of space plasma turbulence from temporal measurements has been one of the major goals of the Cluster mission. For that purpose, techniques, such as the k filtering, have been developed. Such multipoint measurement techniques combine several time series recorded simultaneously at different points in space to estimate the corresponding energy density in wave number space. Here we present results of such an analysis, including a detailed discussion of the errors and limitations that arise due to the separation of the spacecraft and the quality of the tetrahedral configuration. Specifically, we answer the following questions: (1) What are the minimum and maximum scales that can be accurately measured given a specific distance between the satellites? (2) How important is the geometry of the tetrahedron, and what is the relationship of that geometry to spatial aliasing? (3) How should one perform a proper integration of the angular frequencies to infer wave number spectra, and what role does the Doppler shift play when the magnetofluid is rapidly convecting past the spacecraft? We illustrate the results with analyses with both simulated and Cluster magnetometer data recorded in the solar wind. We also discuss the potential impact on future multispacecraft missions, such as Magnetospheric MultiScale and Cross-Scale.

Citation: Sahraoui, F., G. Belmont, M. L. Goldstein, and L. Rezeau (2010), Limitations of multispacecraft data techniques in measuring wave number spectra of space plasma turbulence, *J. Geophys. Res.*, *115*, A04206, doi:10.1029/2009JA014724.

1. Introduction

[2] Analyses of space plasma turbulence from single spacecraft data suffer from the spatiotemporal ambiguity: the difficulty to disentangle temporal variations from spatial ones. Solving this problem has been the major goal of the Cluster mission [Escoubet *et al.*, 1995]. Since its launch in 2000, the Cluster mission has revealed new properties of space plasma turbulence when appropriate data processing techniques, such as the k filtering or the wave telescope are used [Pinçon and Lefeuvre, 1988, 1991, 1992; Neubauer and Glassmeier, 1990]. In the following, we used the term “ k filtering” to refer to either technique since both are, in fact, based on the same mathematical foundation [Pinçon and Motschmann, 1998]. Therefore, all the conclusions and limitations we draw here apply identically to the two methods. The k filtering method is a measurement technique designed for multipoint measurements: it combines several time series recorded simultaneously at different points in space to estimate the energy density in Fourier space, namely, the four-dimensional function $P(\omega, \mathbf{k})$. The basic assumption that underlies the method is that the time series

be sufficiently time stationary and spatially homogeneous. We emphasize that the k filtering *does not* assume any physics about the data under study, such as an existing linear dispersion relation or the weak (or strong) nature of nonlinearities at work. In this sense it is the most general existing method applicable to space plasma turbulence. The method allows one furthermore to include any existing theoretical constraints that might be available, such as the divergence-free equation appropriate for magnetic field fluctuations, viz., $\nabla \cdot \delta \mathbf{B} = 0$. The quantity $P(\omega, \mathbf{k})$, the main product of the k filtering technique, has been used to obtain the three-dimensional (3-D) experimental dispersion relations of low-frequency plasma modes from the magnetic field data in the magnetosheath [Glassmeier *et al.*, 2001; Sahraoui *et al.*, 2003, 2004], in the cusp region [Grisson *et al.*, 2005] and in the magnetotail [Eastwood *et al.*, 2009]. It has been applied to both electric and magnetic field data for the same purpose [Tjulin *et al.*, 2005, 2008]. The method has also been used in an attempt to locate the generation source of waves in space by introducing spherical wave decomposition instead of the plane waves generally used [Constantinescu *et al.*, 2006]. For turbulence studies, Sahraoui *et al.* [2006] have used the k filtering to compute the first 3-D wave number spectrum of low-frequency magnetosheath turbulence by integrating over the angular frequencies $P(\mathbf{k}) = \int P(\omega, \mathbf{k}) d\omega$. Furthermore, reduced wave number spectra $P(k_i) = \int P(k_{i,j,l}) dk_j dk_l$ have been obtained that revealed new anisotropies and scaling laws of magneto-

¹NASA Goddard Space Flight Center, Greenbelt, Maryland, USA.

²Laboratoire de Physique des Plasmas, Ecole Polytechnique Université Pierre et Marie Curie, CNRS, Vélizy, France.

sheath turbulence. A similar approach has been used in a study of turbulence in the foreshock region by *Narita et al.* [2006].

[3] In this paper we apply the techniques to a specific interval of Cluster magnetometer data, but first we present a careful analysis of various sources of error and limitations of the technique. Our discussion includes a careful estimation of the accuracy of the wave number estimation. Another critical issue is how to properly handle spatial aliasing, including the role of the Doppler shift that breaks the (usual) symmetry between determinations of $(\omega_f, -\omega_f)$ and $(\mathbf{k}, -\mathbf{k})$ (in this paper the subscripts “sc” and “f” refer to the spacecraft and the flow reference frames, respectively. For vectors, the subscript “f” refers to the flow direction). The Doppler effect on the frequencies introduces unavoidable anisotropies in the analysis that must be fully understood and dealt with. Although some of these problems have been studied in the original work by *Pinçon and Lefeuvre* [1991, 1992], there is no complete discussion of all of these issues and the literature that has used k filtering tends not to reference to the underlying technical issues. In this paper we illuminate the technical challenges and their solutions using both simulated and real (Cluster) data. In section 2 we discuss how the wave number space is defined given average spacecraft separation; then we will discuss the problem of the spatial aliasing and its relationship with the angular frequencies. We provide the procedure for proper integration of angular frequencies to obtain 3-D wave number spectra, which are those of general interest to turbulence theories. In section 4 we will show the importance of the tetrahedron shape of the Cluster spacecraft and its dramatic impact on the accuracy of the wave number estimation. Finally, we will provide some guidelines that may help in the preparation of the future multi-spacecraft missions such as Magnetospheric MultiScale and Cross-Scale.

2. Small- and Large-Scale Limits on the Wave Number Space

[4] In temporal Fourier analysis, if δt is the sampling time of the time series, then the highest accessible angular frequency (or the Nyquist frequency) is given by $\omega_N = 2\pi/2\delta t$ and all the accessible frequencies belong to $[-\omega_N, \omega_N]$. An antialiasing filter has to be implemented in the hardware of the experiment to filter higher frequencies and thus suppress the aliasing effect. The resolution $\delta\omega$ of the Fourier space, or consequently, the smallest available angular frequency ω_{\min} , is given by $\delta\omega = 2\pi/T$ where T is the total time interval. Practically, the value of T is limited by considerations of time stationarity that are generally required in Fourier analyses.

[5] In the k filtering method the approach is similar, however, the major limitation is that space is probed only in a few points (four in the case of Cluster). Therefore, a careful definition of the accessible k space is required. By analogy with the temporal Fourier analysis, if the average distance between the satellites is d , then the maximum wave number available is $k_{\max} = 2\pi/2d$, and all the accessible scales belong to $[-k_{\max}, k_{\max}]$. However, contrary to the temporal Fourier transform, spatial aliasing cannot technically be avoided as there is obviously no direct way to filter

wave numbers larger than k_{\max} . Therefore, one can only assume that all the wave numbers in the data are smaller than k_{\max} . If wavelengths shorter than the spacecraft separation d exist in the data and propagate undamped past the satellites, aliasing will certainly occur and consequently spurious energy peaks will appear in the wave number domain $[-k_{\max}, k_{\max}]$. In section 3, we will show how to minimize the presence of aliasing.

[6] Given k_{\max} defined above what is the resolution δk to consider? One possible solution would be to infer δk from $\delta k \sim \delta\omega/V_c$, where V_c is a characteristic velocity of the medium (e.g., phase speed of waves or flow speed). However, this estimation suffers from the weakness that it is independent of the spacecraft separation d . And yet one would expect that, given a separation d , the scale $L \sim d$, for instance, will be resolved with a better accuracy than $L \sim 10d$ or $L \sim 100d$ (as we will show below). This leads us to conclude that $k_{\max} \sim \pi/\delta k$, the largest wavelength accessible to measurement, can be obtained only empirically through uncertainty estimation. This estimation has been used by *Sahraoui et al.* [2006], but the rationale was not addressed by those authors. We proceed here to investigate in more detail an approach that works.

[7] Consider the four Cluster satellites located in space at the positions (in kilometers) $\mathbf{r}_1 = 0$, $\mathbf{r}_2 = (10, -47, 80)$, $\mathbf{r}_3 = (-37, -90, 12)$, and $\mathbf{r}_4 = (65, -71, 8)$. These positions reflect good 3-D space coverage enclosing a volume defined by a regular tetrahedron. The planarity (P) and the elongation (E) parameters introduced by *Robert et al.* [1998] are $E \sim P \sim 0.1$, respectively (we discuss the importance of these parameters in section 4). The positions \mathbf{r}_i allows us to calculate the four reciprocal vectors \mathbf{k}_i [*Neubauer and Glassmeier*, 1990; *Sahraoui et al.*, 2003] that define the first Brillouin zone (by analogy with solid state physics), and that satisfy the condition $\sum \mathbf{k}_i = 0$. This fundamental cell has a tetrahedric shape and defines the k space accessible to measurements. When the Cluster tetrahedron is regular the reciprocal cell can be approximated by a cubic-like one (because the sampling is similar along the three directions of space). If, however, the Cluster tetrahedron is not regular, then this approximation is not justified and will lead to spurious results, as we will demonstrate in section 4.

[8] In the example being discussed here, the cubic-like cell has the size $k_{\max} \sim 0.045$ rd/km. The resolution of the k space is arbitrarily fixed to $\delta k = 0.0001$ rd/km. We generate a series of monochromatic plane waves $\mathbf{B}_s \sim \exp[-j(\omega_0 t - \mathbf{k}_s \cdot \mathbf{r}_i)]$ having a fixed angular frequency $\omega_0 = 2\pi f_0$ and different wave vectors $\mathbf{k}_s = (k_s, 0, 0)$ rd/km, where $k_s \in [0.01k_{\max}, k_{\max}]$. This choice allows us to test the capability of the technique to identify scales larger than the satellites separation. In analogy with magnetic field data, we impose the divergence-free condition $\nabla \cdot \mathbf{B} = 0$ on the artificial data, which translates into $\delta \mathbf{B} = (0, \delta B_x, \delta B_z)$ given the choice of the wave vector $\mathbf{k}_s = (k_s, 0, 0)$. We also add 1% of random noise to the data to ensure the existence of the analytical solution $P(\omega, \mathbf{k})$ [*Pinçon and Lefeuvre*, 1991]. As can be seen from the results of the simulation shown in Figure 1, there is a slight difference between the input wave vector k_s and the measured one k_m obtained from the k filtering (given by the maximum of the energy peak). The error $\Delta k_s = |k_s - k_m|$ ranges from δk to $4\delta k$

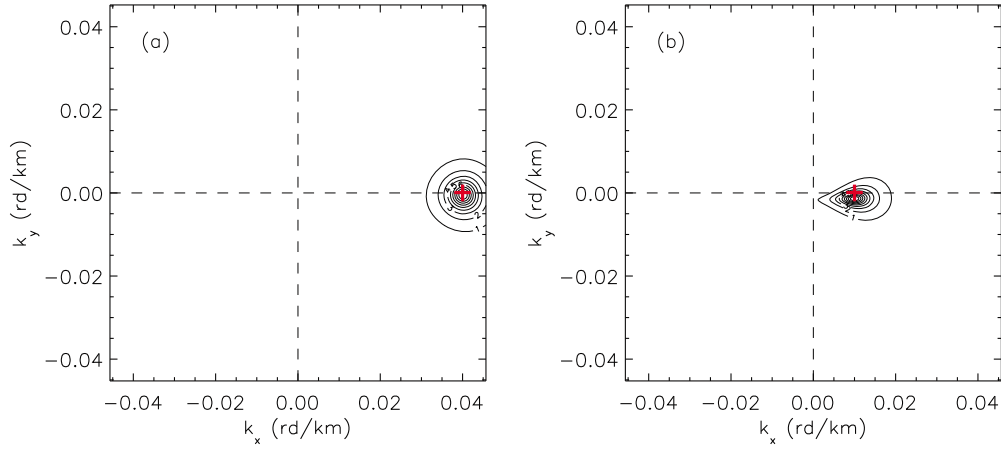


Figure 1. Identification of two simulated plane waves in the plane $k_z = 0$. The waves have wave vectors (a) $\mathbf{k}_1 = (0.0400, 0)$ and (b) $\mathbf{k}_2 = (0.0100, 0)$, denoted by the red crosses. The black curves are isocontours of energy (linearly scaled) obtained from the k -filtering technique. The resolution of the k space is set to $\delta k_x = \delta k_y = 0.0001$ rd/km. The size of the k cell is fixed by the average spacecraft separation d ($k_{x_{\max}} \sim k_{y_{\max}} \sim \pi/d$).

(where $\delta k = 0.0001$ rd/km is the adopted resolution). Consequently, the actual resolution is, at best, ~ 0.0004 rd/km, which is four times larger than the resolution used. The error Δk_s does not improve significantly if the noise level is lowered. Figure 2 shows clearly that the relative errors $\Delta k_s/k_s$ remains very small for scales of the order of the spacecraft separations or larger by about a decade. But the errors significantly increase for scales larger than $10d$ and reach 100% at about $100d$.

[9] Another limitation to the resolution in k space arises from uncertainties in the spacecraft positions. Any error $\Delta \mathbf{r}$ in the positions of the four spacecraft introduces an inaccuracy in the phase determination $\delta \phi = \mathbf{k} \cdot \Delta \mathbf{r}$. The Cluster separations are determined with an accuracy of about 1 km for short separations (~ 100 km). To illustrate this effect we introduce a random error of 5 km in the spacecraft positions. The result (Figure 3) shows a clear shift of the location of the energy peak by about 0.001 rd/km ($\sim 10\delta k$). This sets up a lower limit to the resolution of the k space to be adopted.

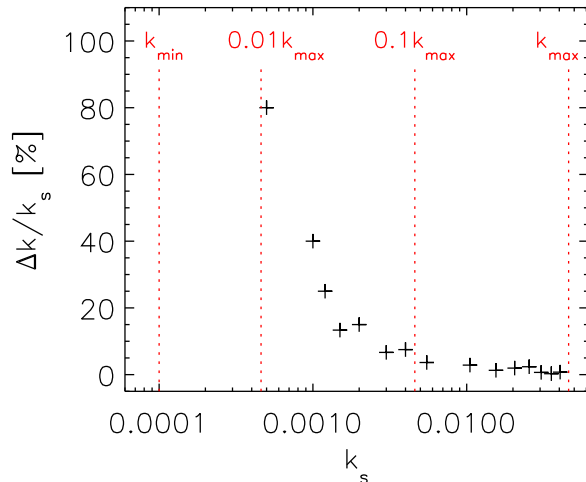


Figure 2. Relative errors $|k_s - k_m|/k_s$ in the determination of the wave vector k_s of the simulated plane waves.

We note finally that other sources of uncertainties may come from the change of the separations and/or the shape of the Cluster tetrahedron over long intervals of time (approximately a few hours). This would occur for instance if one were investigating large-scale solar wind turbulence, where such long data intervals are required.

[10] As a conclusion, given a separation d of the Cluster spacecraft the scales that can be resolved within reasonable error bars ($<10\%$) are, at most, one and a half decades beyond the spacecraft separation d .

3. Spatial Aliasing Problem and Integration of the Angular Frequencies

[11] Aliasing in temporal Fourier analyses is a well-known effect and will not be discussed here. However, the spatial aliasing that occurs using k filtering is consider-

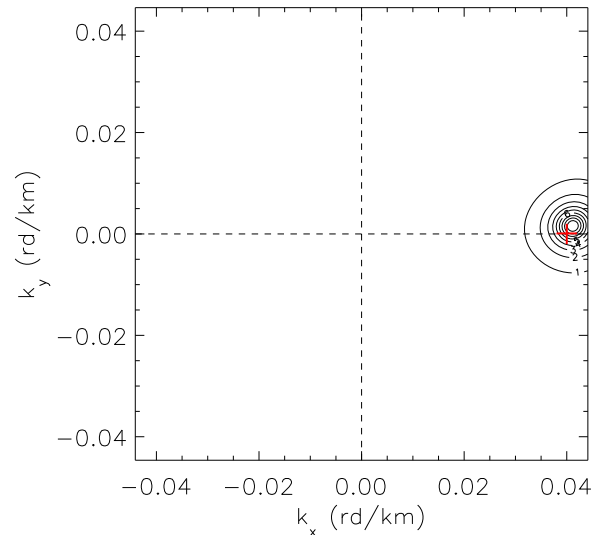


Figure 3. Shift in the measured energy peak from its original location (red cross), as obtained in Figure 1a, due to random errors in the satellite positions of 5 km.

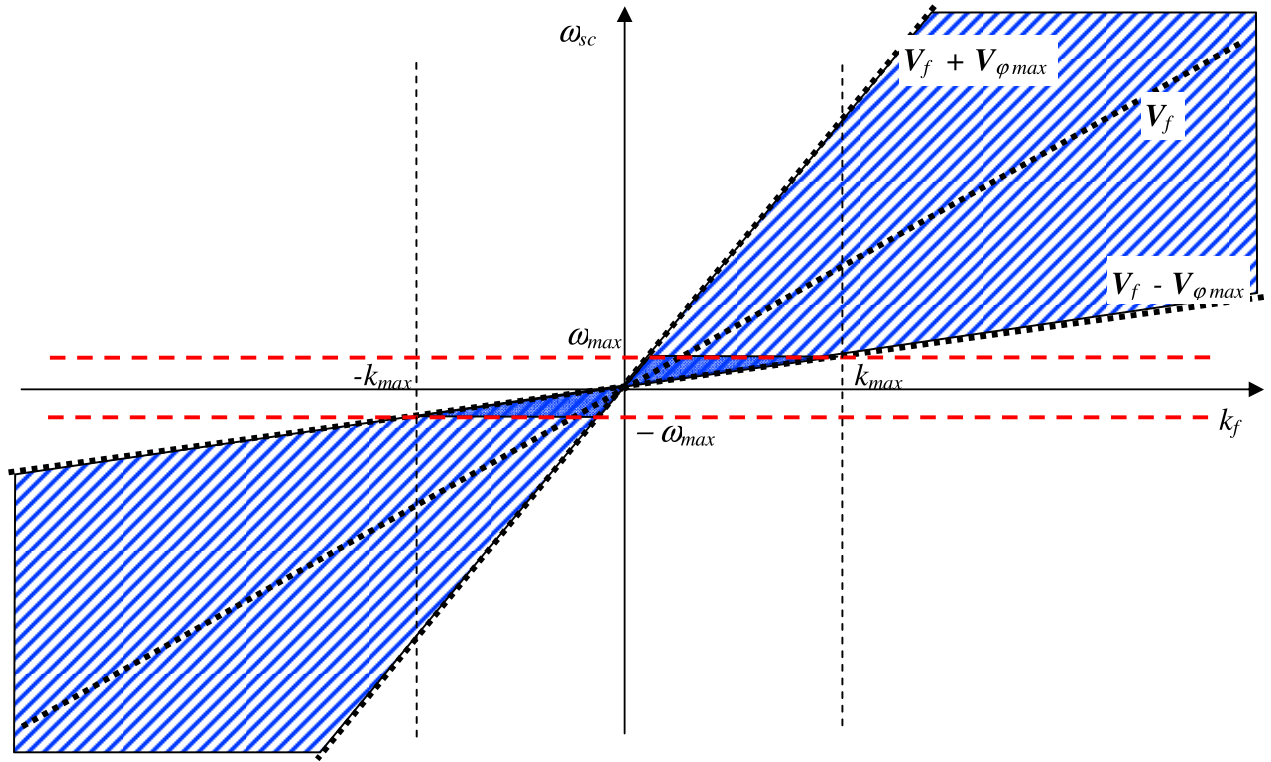


Figure 4. Spacecraft reference frame: Plane $[\omega_{sc}, k_f]$ showing how the limitation in k_f , necessary to avoid spatial aliasing, translates into a limitation in ω_{sc} .

ably more difficult to deal with and, if it is not well understood, can lead to wrong results and biased physical interpretations.

3.1. Spatial Aliasing in the (ω, k) Space

[12] As explained in section 2, the k filtering technique assumes that all fluctuation scales belong to a basic range $[-k_{max}, k_{max}]$, k_{max} being of the order of the inverse interspacecraft distance π/d . Out of this range, i.e., for wave numbers with absolute values larger than k_{max} , all fluctuations would appear as aliased. Fortunately, since the frequency is most generally an increasing function of the wave number, one can show that this problem can be avoided, or limited, by restricting the investigated frequencies to some range $[-\omega_{max}, \omega_{max}]$.

[13] To illustrate this point and to understand its consequences, consider the sketch in Figure 4, where ω_{sc} is the frequency in the spacecraft frame and k_f is the component of \mathbf{k} along the flow direction. Figure 4 possesses a symmetry with respect to the origin. All points, for instance in the third quadrant, represent the same waves as those in the first quadrant because they correspond to the complex conjugate part of the complex Fourier transform versus space and time. It is therefore generally sufficient to consider one half of Figure 4, namely the $\omega_{sc} > 0$ part. With this restriction, the two signs of k_f correspond, if necessary, to the two senses of propagation. The hatched blue region corresponds to all the “possible” waves that can be expected in the plasma. The physical argument is that all these waves have propagation velocities V_{sc} in the spacecraft frame which belong to a range $V_f - V_{\phi max} < V_{sc} < V_f + V_{\phi max}$, where V_f is the flow velocity and $V_{\phi max}$ is the maximum wave

velocity in the flow frame. At low frequencies, in particular (the “MHD” range), where the maximum of energy generally lies, it is known that these intrinsic propagation velocities are always of the order of, or smaller than, the Alfvén and sound velocities: $V_{\phi max} = \text{Max}(V_A, c_s)$. In many situations the propagation velocities are much less than $V_{\phi max}$ (e.g., the slow waves or nonpropagating “waves” such as “mirror modes”). This “natural” limitation leads to the limitation $[-k_{max}, k_{max}]$ necessary to avoid aliasing, at the condition of voluntarily limiting the investigated frequencies to $\omega_{max} = k_{max}(V_f - V_{\phi max})$. This new limitation is marked by the red lines in Figures 4 and 5 and does guarantee results free of aliasing so long as $V_{\phi max}$ has been correctly estimated. An estimate of these limits using solar wind data is given in section 4. We note that the limitations discussed here are due only to considerations of spacecraft separation and plasma flow speed. These limits can moreover be further constrained by consideration of time stationarity and spatial homogeneity.

[14] An important point to highlight here is related to situations where very different phase speeds may coexist in the medium. For instance, in the solar wind the flow speed V_f is generally much higher than the Alfvén or the thermal speed: $V_f \sim 10V_A \sim 10V_{th}$. In this case, the estimation of ω_{max} requires some caution since it depends upon the phase speed and the direction to be considered. Along the flow, for instance $\omega_{max} \sim k_{max}V_f$, is ten times larger than it is in the two directions perpendicular to the flow $\omega'_{max} \sim k_{max}V_A \sim k_{max}V_f/10$. Strictly speaking this latter should be the upper limit to consider to totally avoid spatial aliasing. If, however, ω_{max} is considered instead of ω'_{max} , then aliasing may occur in directions perpendicular to the

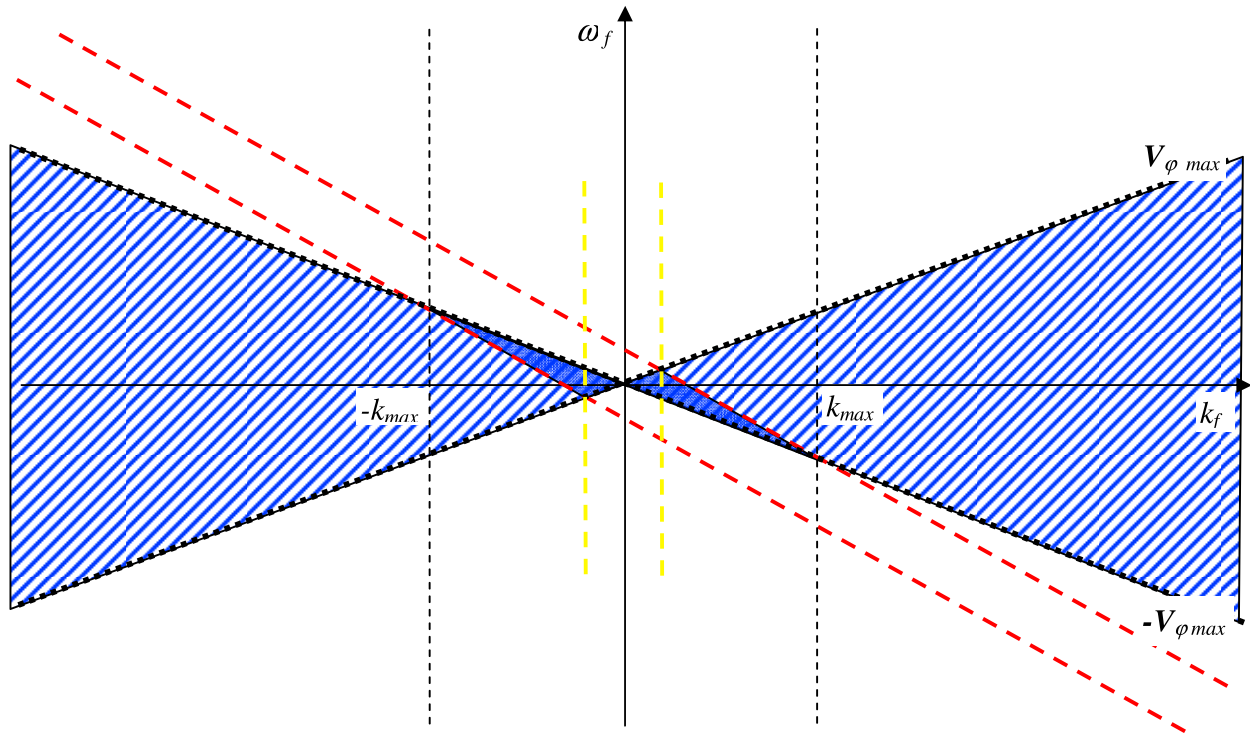


Figure 5. Flow reference frame: Dissymmetric spectra in the plane $[\omega_f, k_f]$ after correcting Figure 4 from the Doppler shift. The yellow lines delimit the region where a proper integration of the angular frequencies ω_f is possible (see text).

flow. The limitation may, however, be relaxed when the wave vectors of the turbulence are not parallel to the flow direction, which may render the two limits ω_{\max} and ω'_{\max} comparable. Indeed, given a finite angle between $\theta = (\mathbf{k}, \mathbf{V}_f)$ the limit $\omega_{\max} = \mathbf{k} \cdot \mathbf{V}_f = kV \cos \theta$ can be of the order of $\omega'_{\max} \sim kV_A$ when $\cos \theta \sim V_A/V_f$.

3.2. Integration of Angular Frequencies and the Doppler Shift

[15] One of the most important quantities that we can calculate from the energy density $P(\omega_{sc}, \mathbf{k})$ is the k spectrum of the turbulence integrated over the angular frequencies ω_f in the flow reference frame, viz., $P'(\mathbf{k}) = \int P(\omega_f, \mathbf{k}) d\omega_f$. To accomplish this, one must understand how the energy density $P(\omega_{sc}, \mathbf{k})$ obtained in the spacecraft frame can be corrected using the Doppler frequency shift to obtain the energy density $P(\omega_f, \mathbf{k})$ in the flow frame. The effect of including the Doppler corrections changes the results shown in Figure 4 to those shown in Figure 5. As is clear from Figure 4, the limit ω_{\max} imposed in the spacecraft frame to avoid spatial aliasing leads to a very significant limitation in the flow frame.

[16] A symmetry does still exist in Figure 4 with respect to the origin. One can consider only the positive frequency half of Figure 4, but it is worth noting that the positive ω_f range in Figure 5 is not the transform of the positive ω_{sc} part of Figure 4. The flow frame result shows that even if waves are isotropically distributed in the hatched blue region, they will be observed to be asymmetric in the flow frame. Typically, for a given ω_f , wave power will be observed over a larger range of k in the negative sense of propagation as compared with the positive propagation direction (in the flow frame).

This asymmetry derives from the flow velocity and arises from the limitation in ω_{sc} imposed to avoid aliasing.

[17] All these issues are important to consider, especially when one attempts to get a k spectrum integrated over frequencies. The integrated k spectrum must be symmetric (even) with respect to k_f as a condition of doing the integration over all (positive and negative) frequencies. This operation, while trivial in the spacecraft frame, is more complicated in the flow frame. In addition, it is clear from Figures 4 and 5 that, for a given k_f , the artificial limit (red lines) brings up an upper limit to the integration that is increasingly restrictive as one approaches the limits $\pm k_{\max}$. This varying width of the accessible range (i.e., it is maximum close to origin and minimum close to k_{\max}) may spoil the integrated spectrum whenever the waves do fill the blue region. The integrated spectrum, as long as one has no more information about the location of the waves in the (ω_{sc}, k_f) plane, is only certain up to a maximum value of k_f , which is of the order of $\omega_{sc}/(V_f + V_{\phi\max})$ (shown by the yellow lines in Figure 5). This limit is noticeably smaller than k_{\max} , and can reach the upper value k_{\max} only in the limit $V_{\phi\max} \rightarrow 0$, i.e., for quasi-stationary plasma modes. For finite phase speed, the region of integration must be restricted to the yellow zone: energy of wave vectors higher than $\omega_{sc}/(V_f + V_{\phi\max})$ is truncated and the resulting k spectrum becomes thus unreliable.

4. Importance of the Tetrahedron Geometry of the Satellites

[18] The tetrahedron formed by the four Cluster spacecraft may change dramatically along a given orbit. The

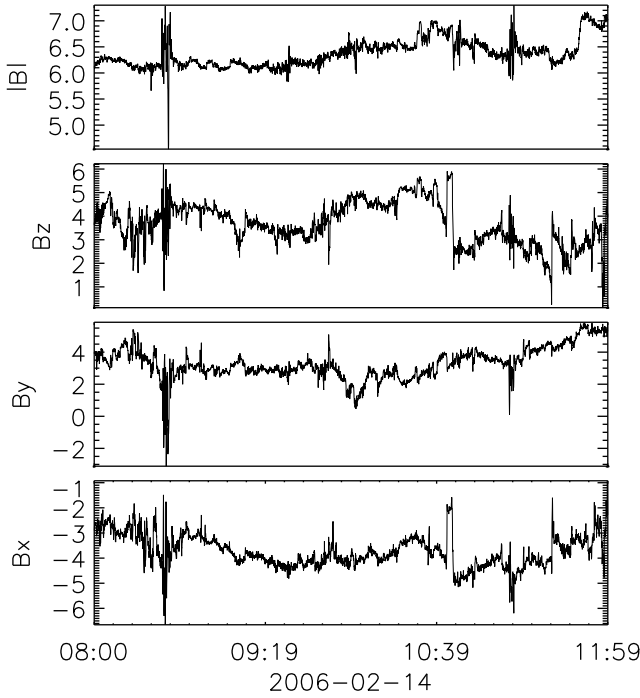


Figure 6. Waveforms measured by FGM in the solar wind in the GSE reference frame.

shape of the tetrahedron is controlled by two parameters, namely the elongation E and the planarity P . $E \sim P \sim 0$ reflects a regular tetrahedron, while $P \sim 1$ and $E \sim 1$ reflect a “cigar” and a “pancake” shape, respectively [Robert *et al.*, 1998]. It is obvious that for the purpose of determining the 3-D properties of the turbulence, a regular tetrahedron is desired. Unfortunately, this requirement has often been ignored. Here we demonstrate by example just how misleading the k spectra obtained from Cluster data can be when the geometry of the tetrahedron is inappropriate.

[19] Consider the magnetic field time series shown in Figure 6. They were recorded in the solar wind on 14 February 2006 from 08h00 to 12h00, by the FGM experiment [Balogh *et al.*, 2001]. At the time the Cluster spacecraft were separated by $d \sim 4 \times 10^3$ km/s. These separation yield average estimated maximum wave vectors $k_{x_{\max}} \sim k_{y_{\max}} \sim k_{z_{\max}} \sim 10^{-3}$ rd/km. During this period the interplanetary magnetic field (IMF) was $B \sim 6$ nT, the plasma density $n_i \sim 9$ cm $^{-3}$, the ion gyrofrequency $f_{ci} \sim 0.1$ Hz, the ion thermal speed $V_{th} \sim 35$ km/s, the Alfvén speed $V_A \sim 45$ km/s, the plasma beta (ratio between ion thermal and magnetic pressures) $\beta_p \sim 0.6$, and the plasma velocity $V_f \sim 320$ km/s. The plasma data are from Cluster Ion Spectrometry (CIS) [Rème *et al.*, 2001]. Using V_f the estimation given in section 3.1 of the upper frequency allowed that avoids the effect of aliasing is $f_{\max} \sim k_{\max} V_f / 2\pi \sim 0.05$ Hz. The smallest measurable wave number with an uncertainty smaller than 10% (section 2) is $k_{\min} \sim k_{\max} / 50$. The resulting minimum frequency in the analysis interval is then $f_{\min} \sim k_{\min} V_f / 2\pi \sim f_{\max} / 50 \sim 10^{-3}$ Hz. These limits are shown in Figure 7, which is the power spectrum of the data in Figure 6. Because FGM data are noisy above 2 Hz [Sahraoui *et al.*, 2009], we superimpose

the spectra using data from the STAFF experiment, which has a better sensitivity at high frequency [Cornilleau-Wehrlin *et al.*, 2003]. The spectra in Figure 7 have two ranges of frequencies with different scalings: a Kolmogorov-like scaling $f^{-5/3}$ for $f < 0.5$ Hz, generally referred to as the inertial range of Alfvénic turbulence and a “dissipation”-like scaling $f^{-4.9}$ for $f > 1$ Hz [Goldstein *et al.*, 1994; Leamon *et al.*, 1998]. These two ranges are separated by a significant bump (also called a “knee” by Alexandrova *et al.* [2006]) centered around the frequency $f \sim 1$ Hz, which is shown to correspond roughly to the Doppler-shifted ion gyroscale or inertial length (one cannot disentangle the two scales because the proton beta $\beta_p \sim 0.6$, Figure 7). We defer further discussion of the physics of the inertial and dissipation ranges for this particular time interval to another paper.

[20] We continue the present discussion by applying the k filtering technique to the frequency $f = 0.03$ Hz taken from the spectra of Figure 7. This frequency is within the interval $[f_{\min}, f_{\max}]$ defined previously. The results are shown in Figure 8, which represents the wave number spectra in the three planes of the k space. The maximum of the energy is centered around the wave vector $\mathbf{k}_0 = (-32, -31, 32) \times 10^{-5}$ rd/km. The most striking aspect of Figure 8 is the stretching of the k spectra in a particular direction in each plane. Is the “anisotropy” physical? In particular, does the high solar wind speed play any role in generating this anisotropy (as may be suggested by the near alignment of the direction of anisotropy with the plasma flow in the planes (k_x, k_y) and (k_x, k_z))? We note however that the orientation of the energy density does not follow the blue curve $\omega_{sc} = \mathbf{k} \cdot \mathbf{V}_f$ (or $\omega_f = 0$), which is expected to govern the Alfvénic turbulence generally observed at these frequencies in the solar wind (since $V_A \ll V_f$) and the mirror mode turbulence in the magnetosheath [Sahraoui *et al.*, 2003, 2006]. Therefore, any departure of the energy peak from the blue curve

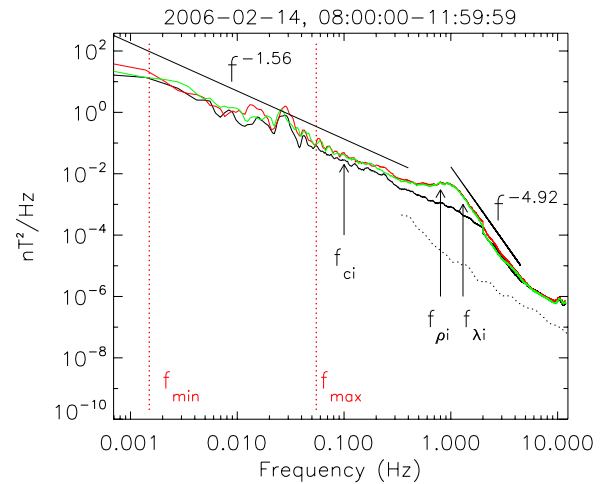


Figure 7. Power spectra of the waveforms shown in Figure 6 from FGM (< 2 Hz) and STAFF (> 2 Hz): B_x (black), B_y (red), and B_z (green). The vertical dotted lines delimit the estimated range of frequencies to which the k filtering can be applied (see text). The vertical arrows are the ion gyrofrequency f_{ci} and the Doppler-shifted ion inertial length $f_{\lambda_i} = V_f / 2\pi \lambda_i$ and ion gyroscale $f_{\rho_i} = V_f / 2\pi \rho_i$.

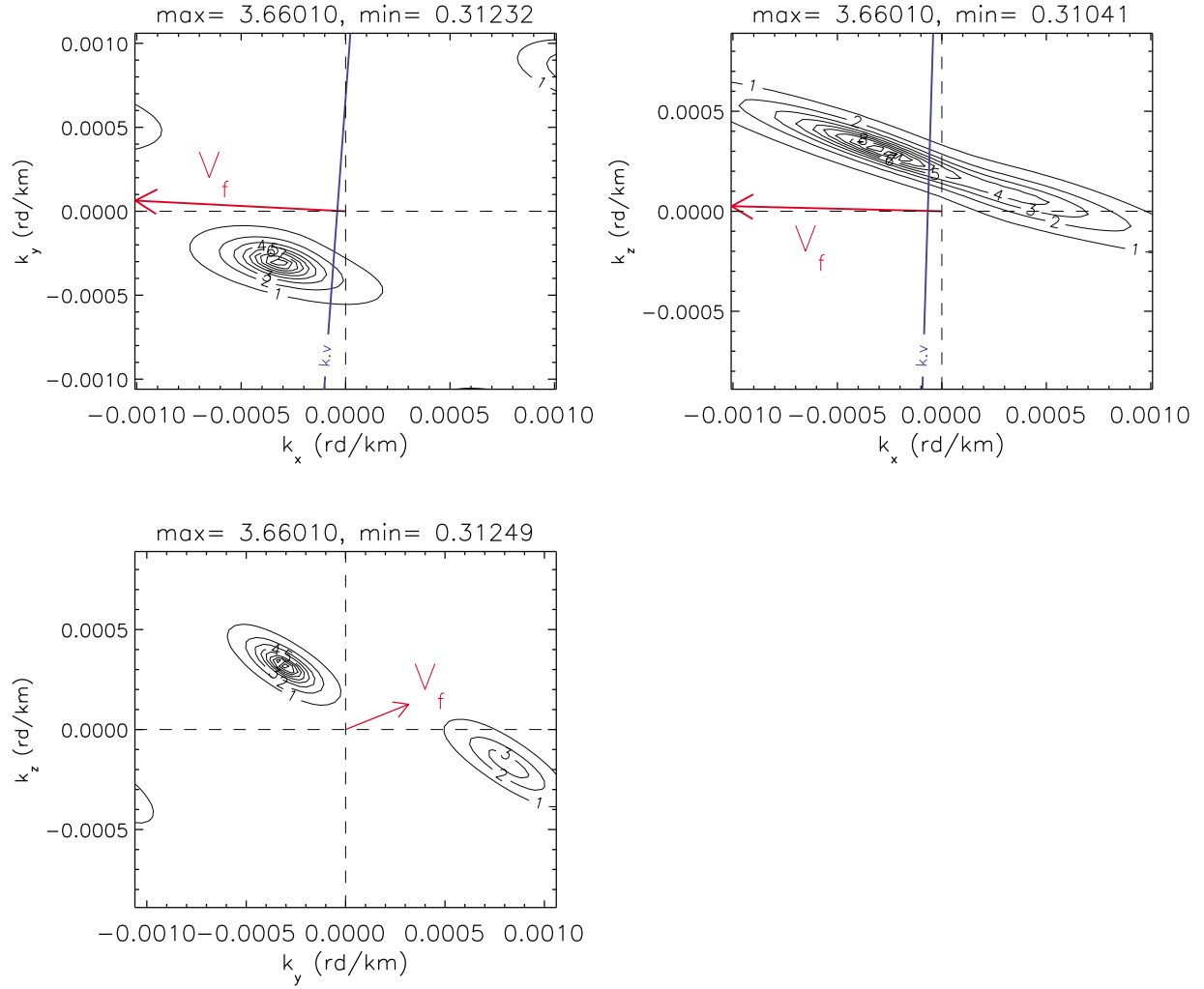


Figure 8. Wave number spectra for the frequency $f = 0.03$ Hz represented in the three planes (k_x, k_y) , (k_x, k_z) , (k_y, k_z) . The blue line is the solution of the equation $\omega_{\text{sat}} = \mathbf{k} \cdot \mathbf{V}_f$. The red arrows are the projections of the flow speed on each plane (the component in the plane (k_y, k_z) is magnified by a factor 5 for the clarity of the plot).

observed here should rise doubts on the validity of the measured k spectra.

[21] To explain the origin of the observed anisotropy, we consider a new simulation using a plane wave with the same wave vector $\mathbf{k} = \mathbf{k}_0$ and the same Cluster tetrahedron as observed in the real data. In this simulation we do not use any flow speed, neither do we introduce any Doppler shift. The simulated plane wave is assumed to propagate past the satellites with a speed $V_\phi = |k_0|/\omega_0$ ($f_0 = \omega_0/2\pi$ being the frequency of the wave). The results are shown in Figure 9. It is remarkable to see how these simulated results reproduce the anisotropies observed in the real data. We can now state unambiguously that the observed anisotropy is purely an artifact caused by the shape of the Cluster tetrahedron. In Figure 9 we have overplotted the projection of the spacecraft positions (rescaled to the size of the k cell). The projection shows that the satellites are strongly elongated along a direction in the $(X_{\text{GSE}}, Z_{\text{GSE}})$ that is perpendicular to the direction of the anisotropy. This stretching is also present in the two other planes, although it is less pronounced. This means that the spacecraft are far from

forming a regular tetrahedron. In fact, the shape is nearly in the $(Y_{\text{GSE}}, Z_{\text{GSE}})$ plane and is slightly elongated in this plane. The planarity P and the elongation E are indeed found to vary over the studied time interval between $[0.65, 1]$ and $[0.55, 0.65]$, respectively, yielding average values $P \sim 0.8$ and $E \sim 0.6$. The main shortcoming of the Cluster geometry at this time is that the direction perpendicular to the pancake or to the cigar is undersampled and that leads to large uncertainties in estimating the wave number spectra in that direction. The uncertainties are smaller (i.e., the energy peaks are less stretched) when the spatial coverage is better (i.e., the surface formed by the projections of the satellites positions is large) as one can see in the plane $(Y_{\text{GSE}}, Z_{\text{GSE}})$ and, to a lesser extent, in $(X_{\text{GSE}}, Y_{\text{GSE}})$. This example illustrates how misleading the k filtering results can be when *all* the conditions of its applicability are not fulfilled.

[22] We emphasize here that this effect is different from the aliasing effect discussed previously. It concerns the large uncertainty in the k vector determination due to an inadequate spatial sampling. The aliasing effect may additionally

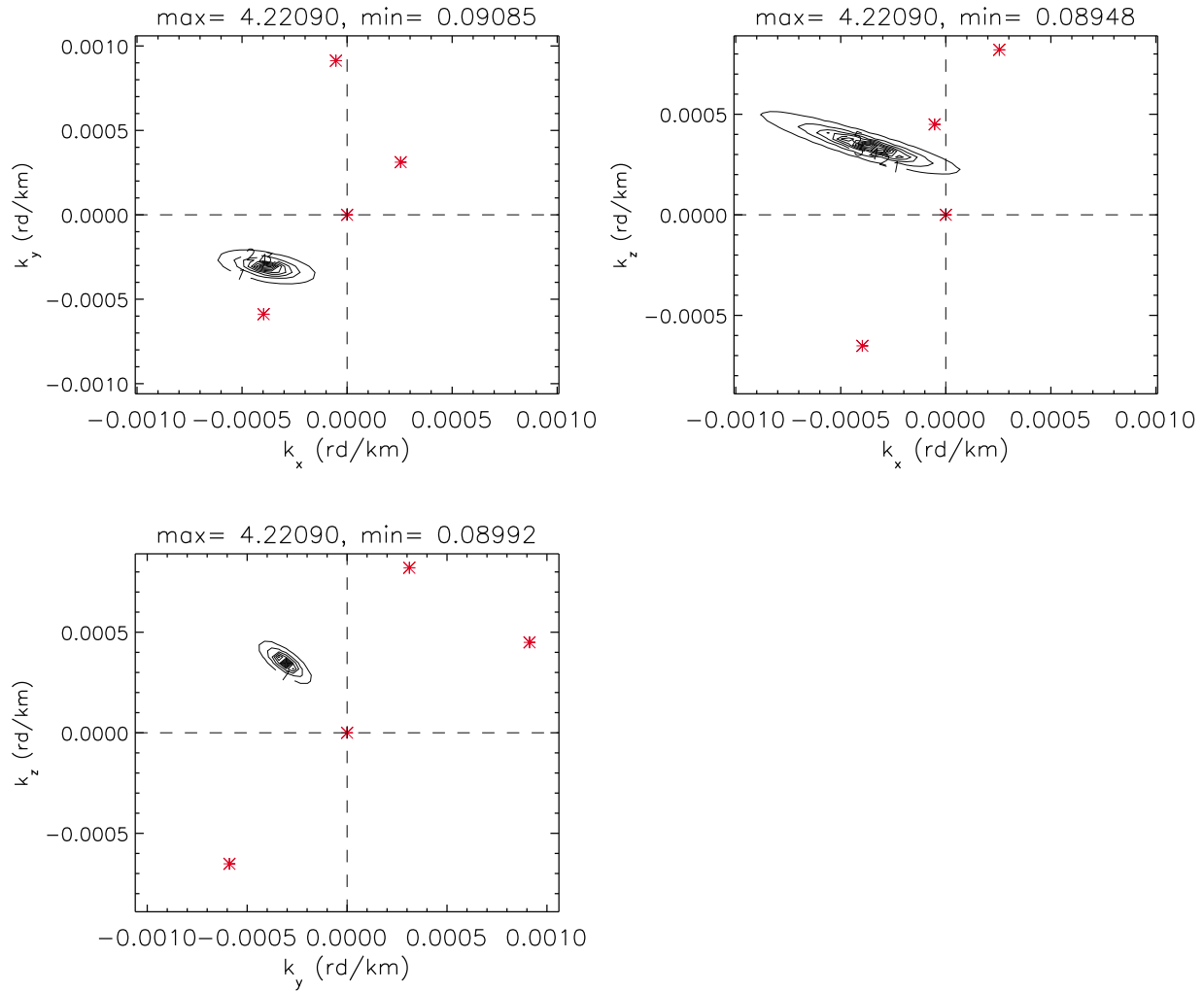


Figure 9. The \mathbf{k} spectra for a simulated plane with $\mathbf{k} = (-32, -31, 32) \times 10^{-5}$ rd/km in the three planes (k_x, k_y) , (k_x, k_z) , (k_y, k_z) calculated using the same tetrahedron as in the real data. The red crosses are the projections of spacecraft positions on each plane (rescaled to the size of the k cell).

come into play and further distort the k spectra [Sahraoui *et al.*, 2003; Tjulin *et al.*, 2005; Narita and Glassmeier, 2009]. This is illustrated in Figure 10, where a spurious peak appears in the fundamental k cell at exactly the same wave number $\mathbf{k}_0 = (5, 5, -9) \times 10^{-4}$ rd/km for both the simulated plane wave and the real data. This procedure of identifying aliased peaks is simpler and more robust than the one introduced by Sahraoui *et al.* [2003]. It is worth noting that the power in this aliased peak is not negligible when compared to that of the first meaningful peak shown in Figures 8 and 9: their ratios are 10% and 30% for the simulated and the real data, respectively. In other cases it is found to be even larger and may reach the level of 100% of the energy maximum. This is an important point, in particular, if one integrates the angular frequencies. Because the level of the spurious peaks is not negligible, the resulting k spectra will not be reliable. We recall finally that in addition to the magnetic field data, electric field data can be used, and one can show that using electric field data can reduce the aliasing problem by the imposition of a new theoretical constraint, viz., Faraday's law, on the measured \mathbf{k} vectors [Tjulin *et al.*, 2005]. But using electric field data does not

fundamentally change the problem: aliasing cannot totally be suppressed. Only satisfying all the requirements that we have discussed in sections 2 and 3 will result in meaningful results that are minimally affected by aliasing and velocity flow distortions.

5. Conclusions

[23] We have presented a study of some important aspects related to the applicability and the limits of using the k filtering method to investigate 3-D properties of space plasma turbulence using simulated and real magnetic field data from the Cluster mission. We have shown that given average spacecraft separation d the scales that can be resolved belong to the interval $[d, 50d]$. The small-scale limit is imposed to avoid aliasing effect, while the large-scale limit ensures that the k vectors are determined with reasonable uncertainties ($<10\%$). We have also shown that restricting the k space to the fundamental cell given by the reciprocal vectors of the satellites positions does not guarantee nonaliased wave vectors and have provided a second limit that must be considered on the angular frequencies. We

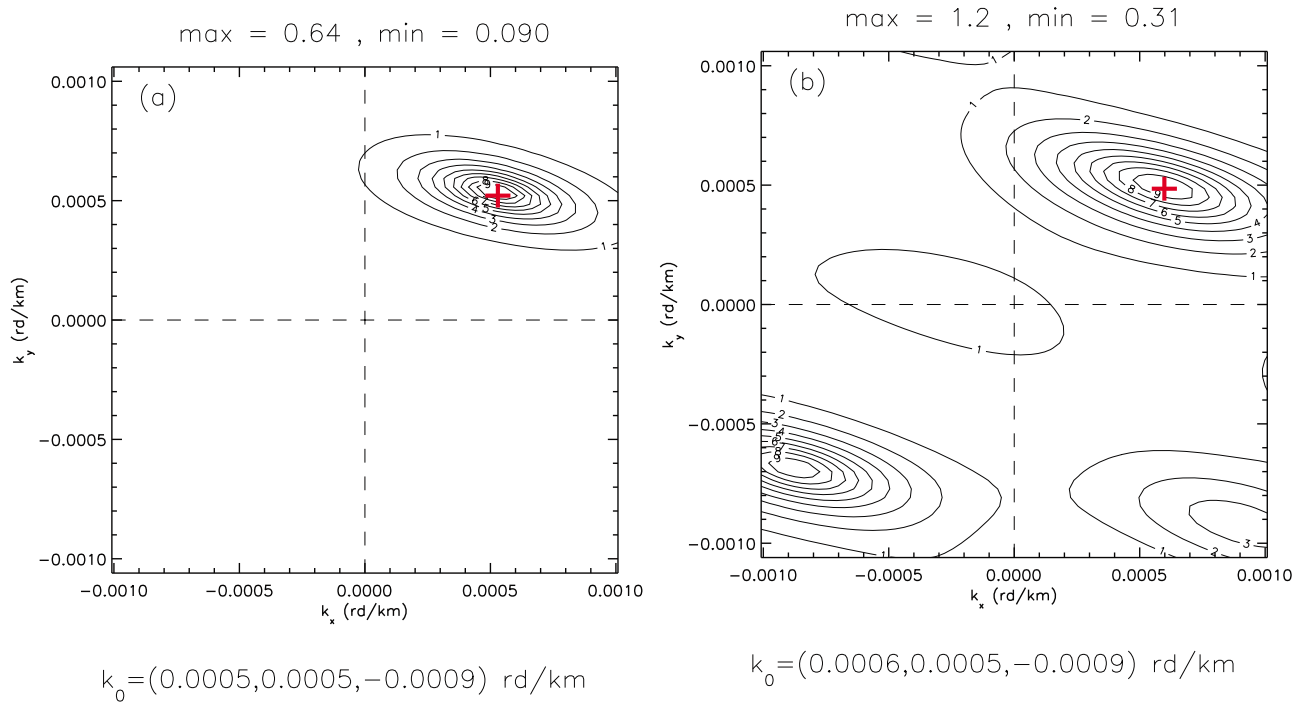


Figure 10. Evidence of an aliased energy peak at the same location (red cross) for (a) the simulated plane wave and (b) the real data.

have discussed the role of the Doppler shift caused by the flow speed on the symmetry breaking of the (ω_f, \mathbf{k}) spectra in the plasma rest frame. We have also described the procedure and the domain of integration of the angular frequencies ω_{sc} that is required to obtain proper \mathbf{k} spectra for comparison with turbulence theories. Finally, we have discussed the role of the tetrahedron geometry on the interpretation on the results of the k filtering and have shown that a regular tetrahedron is *necessary* to retrieve useful results.

[24] The present work highlights two important points relevant to planning future multispacecraft missions: The first one is the necessity of trying to achieve a regular tetrahedral (or other geometrical) configuration in the areas of scientific interest. The second consequence, particularly relevant to the Cross-Scale mission, is the spacecraft separations that needed to be chosen for the mission. For example, if the separations of the inner four satellites is set to 10 km, the medium and outer satellites need to be separated by less than 500 km and 10,000 km, respectively, for turbulence studies. We note that each quartet of satellites will resolve only one range of scales at once (a decade and half at best). One cannot use all the 12 satellites (in the optimal case) to resolve scales with a better accuracy than with four unless all the satellites have comparable separations. If, for example, the outer satellites are separated by a distance $D \sim 5000$ km, considering data from an inner satellite separated by a $d \sim 10$ km from the outer ones will produce higher uncertainty on scales of 10,000 km than if it were computed from the outer satellites alone [Pinçon and Lefeuvre, 1992]. More than four satellites at comparable separations will however provide wave number spectra with a better accuracy than is at present available with Cluster.

[25] **Acknowledgments.** F. Sahraoui would like to thank Jean-Louis Pinçon for stimulating discussions over the last few years of a fruitful collaboration. The FGM data used in this work come from the Cluster Active Archive (ESA), the CIS data from AMDA (CESR, Toulouse, France), and the STAFF data from REPROC (P. Robert, LPP, Vélizy, France). The French participation in the Cluster mission is supported by CNES. F. Sahraoui is partly funded through the NPP program at NASA/GSFC.

[26] Amitava Bhattacharjee thanks the reviewers for their assistance in evaluating this paper.

References

- Alexandrova, O., A. Mangeney, M. Maksimovic, N. Nornilleau-Wehrlin, J.-M. Bosqued, and M. André (2006), Alfvén vortex filaments observed in magnetosheath downstream of a quasi-perpendicular bow shock, *J. Geophys. Res.*, **111**, A12208, doi:10.1029/2006JA011934.
- Balogh, A., et al. (2001), The Cluster magnetic field investigation: Overview of in-flight performance and initial results, *Ann. Geophys.*, **19**, 1207–1217.
- Constantinescu, O. D., K.-H. Glassmeier, U. Motschmann, R. A. Treumann, K.-H. Fornacon, and M. Franz (2006), Plasma wave source location using CLUSTER as a spherical wave telescope, *J. Geophys. Res.*, **111**, A09221, doi:10.1029/2005JA011550.
- Cornilleau-Wehrin, , et al. (2003), First results obtained by the Cluster STAFF experiment, *Ann. Geophys.*, **21**, 437–456.
- Eastwood, J. P., T. D. Phan, S. D. Bale, and A. Tjulin (2009), Observations of turbulence generated by magnetic reconnection, *Phys. Rev. Lett.*, **102**, 035001, doi:10.1103/PhysRevLett.102.035001.
- Escoubet, P., et al. (1995), *The Cluster and Phoenix Missions*, Kluwer Acad., Dordrecht, Netherlands.
- Glassmeier, K.-H., et al. (2001), Cluster as a wave telescope—First results from the fluxgate magnetometer, *Ann. Geophys.*, **19**, 1439–1447.
- Goldstein, M. L., M. D. Roberts, and C. Fitch (1994), Properties of the fluctuating magnetic helicity in the inertial and dissipation ranges of solar wind turbulence, *J. Geophys. Res.*, **99**, 11,519–11,538.
- Grisson, B., F. Sahraoui, B. Lavraud, T. Chust, N. Cornilleau-Wehrin, H. Rème, A. Balogh, and M. André (2005), Wave particle interactions in the high-altitude polar cusp: A Cluster case study, *Ann. Geophys.*, **23**, 3699–3713.
- Leamon, R. J., C. W. Smith, N. F. Ness, W. H. Matthaeus, and H. K. Wong (1998), Observational constraints on the dynamics of the interplanetary magnetic field dissipation range, *J. Geophys. Res.*, **103**, 4775–4787.

- Narita, Y., and K.-H. Glassmeier (2009), Spatial aliasing and distortion of energy distribution in the wave vector domain under multi-spacecraft measurements, *Ann. Geophys.*, *27*, 3031–3042.
- Narita, Y., K.-H. Glassmeier, and R. A. Treumann (2006), Wave-number spectra and intermittency in the terrestrial foreshock region, *Phys. Rev. Lett.*, *97*, 191101, doi:10.1103/PhysRevLett.97.191101.
- Neubauer, F. M., and K. H. Glassmeier (1990), Use of an array of satellite as a wave telescope, *J. Geophys. Res.*, *95*, 19,115–19,122.
- Pinçon, J. L., and F. Lefeuvre (1988), Characterization of a homogeneous field turbulence from multipoint measurements, *Adv. Space Res.*, *8*(9), 459–462.
- Pinçon, J. L., and F. Lefeuvre (1991), Local characterization of homogeneous turbulence in a space plasma from simultaneous measurements of field components at several points in space, *J. Geophys. Res.*, *96*, 1789–1802.
- Pinçon, J. L., and F. Lefeuvre (1992), The application of the generalized Capon method to the analysis of a turbulent field in space plasma: Experimental constraints, *J. Atmos. Terr. Phys.*, *54*, 1237–1247.
- Pinçon, J. L., and U. Motschmann (1998), Multi-Spacecraft filtering: General framework, in *Analysis Methods for Multi-Spacecraft Data*, *ISSI Sci. Rep.*, *SR-001*, pp. 65–78, Int. Space Sci. Inst., Bern.
- Rème, H., et al. (2001), First multispacecraft ion measurements in and near the Earth's magnetosphere with the identical Cluster ion spectrometry (CIS) experiment (2001), *Ann. Geophys.*, *19*, 1303–1354.
- Robert, P., A. Roux, C. C. Harvey, M. W. Dunlop, P. W. Daly, and K. H. Glassmeier (1998), Tetrahedron geometric factors, in *Analysis Methods for Multi-Spacecraft Data*, *ISSI Sci. Rep.*, *SR-001*, pp. 323–348, Int. Space Sci. Inst., Bern.
- Sahraoui, F., et al. (2003), ULF wave identification in the magnetosheath: The k-filtering technique applied to Cluster II data, *J. Geophys. Res.*, *108*(A9), 1335, doi:10.1029/2002JA009587.
- Sahraoui, F., G. Belmont, J. L. Pinçon, L. Rezeau, A. Balogh, P. Robert, and N. Cornilleau-Wehrin (2004), Magnetic turbulent spectra in the magnetosheath: New insights, *Ann. Geophys.*, *22*, 2283–2288.
- Sahraoui, F., G. Belmont, L. Rezeau, N. Cornilleau-Wehrin, J. L. Pinçon, and A. Balogh (2006), Anisotropic turbulent spectra in the terrestrial magnetosheath as seen by the Cluster spacecraft, *Phys. Rev. Lett.*, *96*, 075002, doi:10.1103/PhysRevLett.96.075002.
- Sahraoui, F., M. L. Goldstein, P. Robert, and Y. V. Khotyaintsev (2009), Evidence of a cascade and dissipation of solar-wind turbulence at the electron gyroscale, *Phys. Rev. Lett.*, *102*, 231102, doi:10.1103/PhysRevLett.102.231102.
- Tjulin, A., J. L. Pinçon, and F. Sahraoui (2005), The k-filtering technique applied to wave electric and magnetic field measurements from the Cluster satellites, *J. Geophys. Res.*, *110*, A11224, doi:10.1029/2005JA011125.
- Tjulin, A., E. A. Lucek, and I. Dandouras (2008), Wave activity inside hot flow anomaly cavities, *J. Geophys. Res.*, *113*, A08113, doi:10.1029/2008JA013333.
- G. Belmont and L. Rezeau, Laboratoire de Physique des Plasmas, Ecole Polytechnique Université Pierre et Marie Curie, CNRS, 10-12 Ave. de l'Europe, F-78140 Vélizy, France. (gerard.belmont@lpp.polytechnique.fr; laurence.rezeau@lpp.polytechnique.fr)
- M. L. Goldstein and F. Sahraoui, NASA Goddard Space Flight Center, Code 673, Greenbelt, MD 20771, USA. (melvyn.l.goldstein@nasa.gov; foud.sahraoui-1@nasa.gov)